Turk J Chem
35 (2011) , 735 – 743.
© TÜBİTAK
doi:10.3906/kim-1103-50

Electrochemical impedance spectroscopy study on intercalation and anomalous diffusion of $AlCl_4^-$ ions into graphite in basic molten salt

Ali EHSANI, Mohammad Ghasem MAHJANI*, Majid JAFARIAN
Department of Chemistry, Faculty of Science, K.N. Toosi University of Technology, P. O. Box 15875-4416, Tehran-IRAN
e-mail: mahjani@kntu.ac.ir

Received: 27.03.2011

Electrochemical impedance spectroscopy (EIS) was employed to investigate diffusion of $AlCl_4^-$ ions in basic ($AlCl_3$-NaCl-KCl) molten salt. Nyquist plots in different DC offset potentials showed finite and restricted aluminum ion diffusion due to insertion and blocking in the graphite electrode. The general Warburg, open Warburg, and short Warburg impedance in the complex Nyquist plot of this system showed the anomalous diffusion behavior of the ions in the graphite electrode. The diffusion coefficient of the $AlCl_4^-$ ions was calculated from the slope of the Warburg line in a totally blocking film in the graphite electrode and was found to be 2.8×10^{-10} cm^2/s.

Key Words: Aluminum chloride, molten salt, impedance, anomalous diffusion

Introduction

Electrochemical impedance spectroscopy (EIS) is one of the most universal and powerful electroanalytical techniques for the fine characterization of chemical kinetics and transport processes occurring in thin-coated and ion-insertion electrodes. Boundary conditions have a strong influence on the control of diffusion processes in electrochemical systems. For these systems, with mobile ions, diffusion flux implies a Warburg-like impedance; this impedance is a $\omega^{1/2}$ function.

$$Z(i\omega) \propto (i\omega)^{-1/2} \quad (1)$$

*Corresponding author

However, in many cases, impedance measurements of diffusive processes give rise to power laws in frequencies that deviate more or less from the exact $^1/_2$-exponent law in Eq. (1).

$$Z(i\omega) \propto (i\omega)^{-\beta/2} \quad (0 < \beta < 2), \tag{2}$$

where ω is the angular frequency of the external electric field. The Warburg-like impedance can be calculated from Fick's laws of diffusion for a process with a vanishing relaxation time,[1] or from a generalized diffusion equation for processes with a nonvanishing relaxation time.[2] The selective nature of borders and the diffusion length are very important in determining the Warburg impedance from Fick's equation or from a generalized diffusion equation. Usually, the solutions of these problems are limited only to semiinfinite boundary conditions.[3] However, the boundary conditions for real electrochemical systems are neither totally transmissive nor reflective conditions; the borders of real systems show a partially transmissive or reflective nature. Analyzing the Nyquist plot in impedance spectra is one of the best techniques for monitoring some of the changes occurring within intercalation compounds during insertion and extraction.

The aim of this paper was to calculate, in the framework of extended irreversible thermodynamics,[4] Warburg-like impedance for an electrochemical molten system ($AlCl_3$-NaCl-KCl) with generalized boundary conditions for processes with a nonvanishing relaxation time into the graphite electrode. In view of the application, a few preliminary reports showed that carbon nanotubes can also be produced in the liquid phase by molten salt electrolysis at mild temperatures. The graphite intercalation of alkali metal plays an important role in the formation of the electrolytic carbon nanotubes.[5,6] The low temperature of this eutectic is appropriate for this application.

Experimental

Materials used in this work were of analytical grade, from Merck. $AlCl_3$ was redistilled while NaCl and KCl were dried at 300 °C prior to use. The fused electrolyte, with a composition of 66:20:14 wt.% ($AlCl_3$-NaCl-KCl) that was equivalent to 48.2:33.4:18.4 mol%, had a melting point starting at around 115 °C and terminating at nearly 120 °C as measured in our laboratory. The molten electrolyte was a 1-phase clear liquid at 140 °C, the temperature at which the electrochemical studies were performed. The handling of the materials and the procedures concerning the preparation of the fused electrolyte were much the same as reported elsewhere.[7–9]

The experiments were carried out at 140 °C in a conventional 3-electrode cell with a hand-polished graphite rod, with a surface area of 0.22 cm^2 forming the working electrode. Its potential was monitored against a Ag/AgCl electrode placed inside the melt. A large graphite rod was used as the counter electrode. The electrochemical cell was powered by an EG&G 273A potentiostat/galvanostat coupled with a Solartron 1255 frequency response analyzer run by a PC with M270 and M398 commercial software. The frequency range of 100 kHz to 10 mHz and a modulation amplitude of 5 mV were employed for the impedance studies. The electrical impedance was calculated without subtracting the uncompensated resistance or the double-layer capacitance. Fitting of the experimental data to the proposed theoretical models was done by means of home-written least square software based on the Marquardt method for optimization of functions and Macdonald weighting for the real and imaginary parts of the impedance.[1]

Results and discussion

Figure 1 presents a cyclic voltammogram obtained in the potential range of -0.6 to -1.5 V vs. Ag/AgCl at 140 °C without IR drop correction. The electroactive entity, probably $AlCl_4^-$, started to reduce at -1.1 V vs. Ag/AgCl according to following reaction: $AlCl_4^- + 3e^- \rightarrow Al + 4Cl^-$.

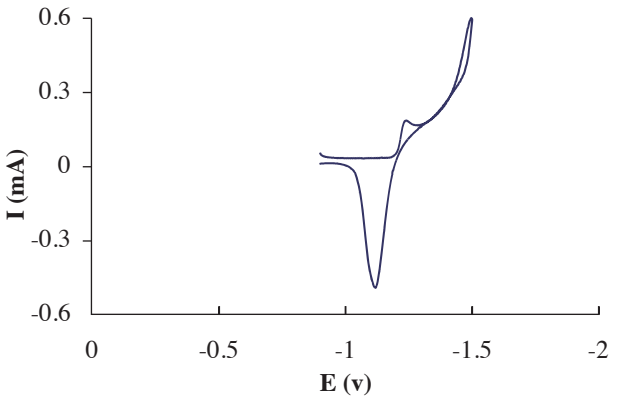

Figure 1. Cyclic voltammogram of the graphite electrode in basic molten salt (140 °C) at a scan rate of 100 mV/s.

Figures 2-5 present complex plane plots and equivalent circuits recorded at various applied cathodic potential steps in the range of -1.14 to -1.22 V vs. Ag/AgCl. At high frequency, the distorted capacitive loop is related to the charge transfer resistance for one-step reduction of $AlCl_4^-$ in parallel with double-layer capacitance. At low frequency, semiinfinite and finite Warburg impedances were observed, which are characteristics of the insertion and blocking of aluminum ions. The processes give rise to changes in the active area of the substrate surface.

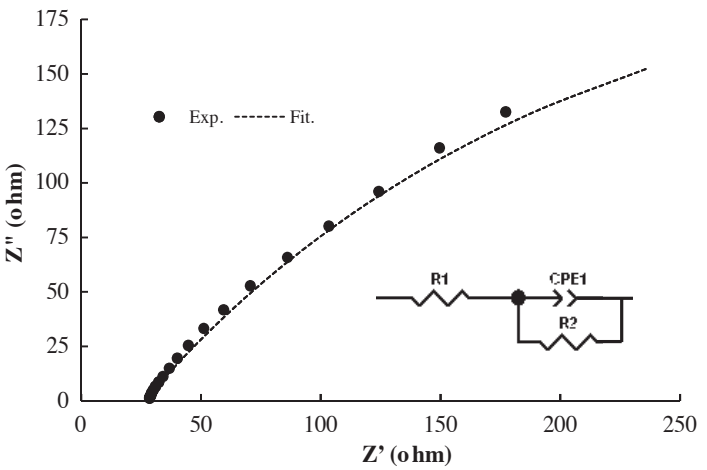

Figure 2. Nyquist plot and equivalent circuit for double-layer capacitance of $AlCl_4^-$ anions at DC offset potential –1.14 V (R_1 = 26.62 ohm, CPE-T = 40.55 × 10^{-5} F, n = 0.59, R_2 = 693.7 ohm).

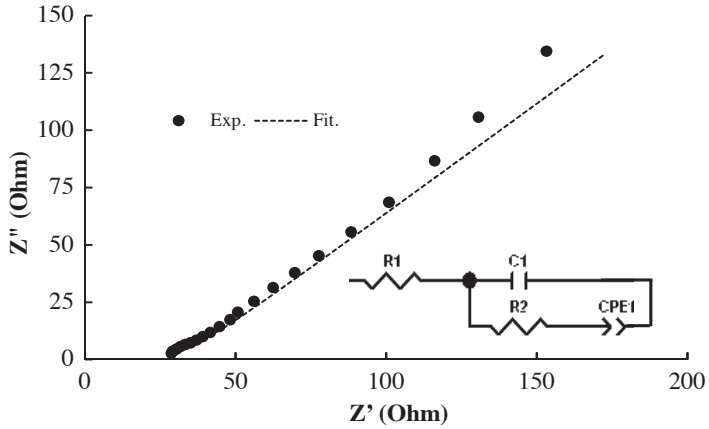

Figure 3. Nyquist plot and equivalent circuit for ordinary diffusion of $AlCl_4^-$ anions at DC offset potential–1.16 V (R_1 = 27.64 ohm, $C_1 = 4.09 \times 10^{-6}$ F, R_2 = 7.68 ohm, CPE-T = 1.71×10^{-3}, n = 0.49).

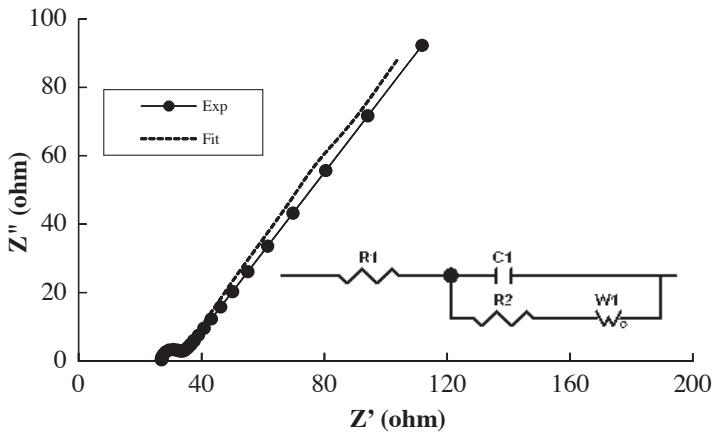

Figure 4. Nyquist plot and equivalent circuit for diffusion of $AlCl_4^-$ anions with a totally blocking boundary condition at DC offset potential –1.18 V (R_1 = 24.48 ohm, $C_1 = 4.24 \times 10^{-7}$ F, R_2 = 2.8 ohm, W1-R = 20.12 ohm, n = 0.55, W1-T = 0.65).

EIS can access relaxation phenomena over many orders of magnitude and has been employed for the study of the kinetics of the charge-transfer process into and across electroreactive films.[10–12]

The processes that occurred in the course of the redox transition of the film are a combination of electron transfer at the film/solution interface, slow diffusion of interstitial ions in the solid lattice of film, flip-flopping of ions across the film/solution interface, and fast ion transport in the bulk of the solution.[13,14] Accordingly, the Faradaic current, which passes through the film/solution interface, is a function of $AlCl_4^-$ ion concentration, and the potential at this interface and the 2 potential steps of δE_1 through the film and δE_2 at the film/solution interface dominate. The electrochemical impedance Z_f is calculated as the ratio of potential to current under a small perturbation of potential. Therefore, the Faradaic impedance is

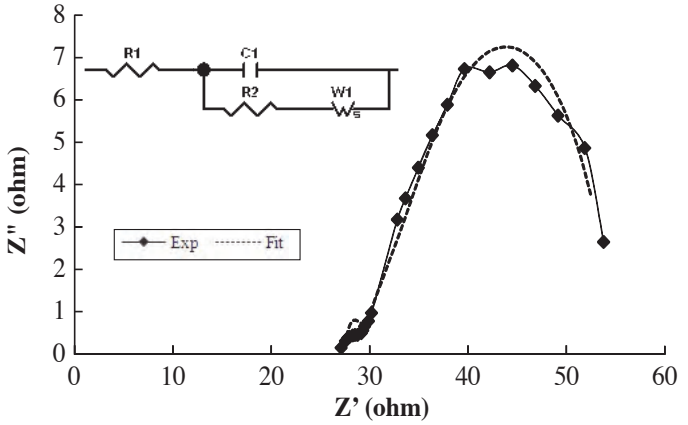

Figure 5. Nyquist plot and equivalent circuit for diffusion of $AlCl_4^-$ anions with a totally absorbing boundary condition at DC offset potential –1.22 V (R_1 = 27.53 ohm, $C_1 = 5.72 \times 10^{-6}$ F, R_2 = 1.12 ohm, W1-R = 26.42 ohm, n = 0.37, W1-T = 0.76).

$$Z_f = \frac{\delta E_1}{\delta I_f} + \frac{\delta E_2}{\delta I_f}, \tag{3}$$

and the flux of charged species at the film/solution interface, using the Taylor series expansion and the Laplace transform, is[14]

$$\frac{\delta J_{ion}}{\delta E_2} = \frac{\xi_{ion}}{1 + \zeta_{ion}\left[\coth\left[d(j\omega/D_{ion})^{0.5}\right]/(j\omega D_{ion})^{0.5}\right]}. \tag{4}$$

In this equation

$$\xi_{ion} = b^1_{ion}, K^1_{ion}(C_{ion} - C_{ion,\min}) - C_{ion,sol}b^{-1}_{ion}K^{-1}_{ion}(C_{ion,\max} - C_{ion}), \tag{5}$$

$$\zeta_{ion} = K^1_{ion}\exp\left[b^1_{ion}(E - E^0)\right]K^{-1}_{ion}\exp\left[b^{-1}_{ion}(E - E^0)\right]C_{ion,sol} \tag{6}$$

where the subscript ion represents the solid-state diffusing ion. Meanwhile, d is the mean diffusion length equal to the thickness of the graphite, D_{ion} is the diffusion coefficient of $AlCl_4^-$ ions through the film, ω is the angular frequency of the AC of the imposed sinusoidal signal, $j = \sqrt{-1}$, and E_0 is the formal potential. $C_{ion,min}$ and $C_{ion,max}$ are the minimum concentration of the sites occupied by the species in the host film and the maximum concentration of the sites available for insertion of $AlCl_4^-$ ions into the film structure, respectively. $C_{ion,soln}$ is the ion concentration in the bulk of solution, C_{ion} is the concentration of occupied sites in the film, and K^1_{ion} and K^{-1}_{ion} are the kinetic rate constants of the transfers, which are dependent on potential. In these equations, ξ is negative/positive for the insertion/deinsertion of $AlCl_4^-$ ions. The films of graphite have very thin thicknesses and, therefore, ∂E_1 is negligible in comparison with ∂E_2. Thus, Eq. (3) for Faradaic impedance is reduced to

$$Z_f = \frac{\delta E_2}{\delta I_f} = \frac{1}{F\xi_{ion}}\left\{\frac{1 + (\zeta_{ion}\tau_{ion}\coth(j\omega\tau_{ion})^{0.5}}{d(j\omega\tau_{ion})^{0.5}}\right\}, \tag{7}$$

where $\tau_{ion} = d^2/D_{ion}$ is the time constant of the diffusion process. Another approach that can be used to interpret the impedance response is the model of the wave transmission in a finite-length RC transmission

line,[15] which was used for a porous electrode or an electroreactive film.[16] In this expression, the Faradaic impedance is

$$Z_f = R_{ct} + Z_{FLW} = R_{ct} + R_{FLW}\left\{ctnh(\frac{(j\omega R_{FLW}C_{FLW})^{0.5}}{(j\omega R_{FLW}C_{FLW})^{0.5}}\right\}, \tag{8}$$

where R_{ct} is the charge-transfer resistance, R_{FLW} analogizes the resistance of the diffusion of a species through a finite length, and C_{FLW} describes the capacitance of the finite space. By comparing Eqs. (7) and (8), the following can be deduced.

$$\tau_{ion} = R_{FLW}C_{FLW} = \frac{d2}{D_{ion}} \tag{9}$$

$$\frac{d}{\zeta_{ion}\tau_{ion}} = \frac{R_{ct}}{R_{FLW}} \tag{10}$$

$$\xi_{ion} = \frac{1}{FR_{ct}} \tag{11}$$

As the bias of the system is systematically varied, different signatures were observed in the Nyquist diagrams and different processes dominated the electrochemical characteristics of the film. These behaviors were modeled by the dominance of different components in electrical equivalent circuits. The Nyquist diagrams are better interpreted if constant phase elements (CPEs) are replaced with the pure capacitances in an inhomogeneous surface. The impedance of these elements is[17]

$$Z_{CPE} = \frac{1}{T_0(j\omega)^n}, \tag{12}$$

where T_0 is the CPE coefficient and n is the CPE exponent. For perfect capacitance, n is equal to unity.

In the Nyquist diagram recorded at the DC potential of –1.14 V (Figure 2), a capacitive depressed semicircle appeared. The DC potential of –1.14 V is around the potential of the cathodic peak of $AlCl_4^-$ reduction. The Nyquist plot in Figure 2 shows the formation of double-layer capacitance with a charge-transfer resistance of $AlCl_4^-$ anions in the working electrode surface at DC offset potential –1.14 V vs. Ag/AgCl. An electrical equivalent circuit model was employed for the analysis of this Nyquist diagram, which is shown in the inset of Figure 2. The fitted Nyquist diagram using this equivalent circuit is also shown. In this circuit, R_1, CPE_{dl}, and R_2 are the solution resistance, a CPE that describes the double-layer capacitance, and the charge-transfer process of an aluminum redox couple, respectively.

At the DC potential of –1.16 V (Figure 3), the diameter of the high-frequency semicircle is lowered. This is due to the potential dependency of the charge-transfer process of aluminum species at the graphite surface. One additional signature is starting at very low frequencies for the ordinary diffusion of aluminum species. At the DC potential of –1.18 V (Figure 4), a similar pattern to that observed at –1.16 V was noted; the diameter of the semicircles is thus decreased and the very-low-frequency response is revealed to be a capacitive response. This near-vertical line at low frequency is related to the well-known redox capacitance behavior of graphite film.[18] The electrical equivalent circuit compatible with the Nyquist diagrams is shown in the inset of Figure 4 and the fitted Nyquist diagrams using this equivalent circuit are represented. In this circuit, R_1, C_1, and R_2 are the solution resistance, double-layer capacitance, and charge-transfer process of an aluminum redox couple,

respectively. Meanwhile, Wo is the open-circuit terminus Warburg element. The values of the electrical element components of this equivalent circuit were obtained by a fitting procedure and are reported in Figure 4.

The slope of the linear tail at high frequencies is higher than a pure Warburg line (unity), and that at low frequencies is lower than pure capacitance (infinity). However, based on Eq. (8), the theoretical impedance response should be a line with a slope of unity followed by a vertical line, or open-circuit terminus Warburg impedance. Therefore, both parts of the impedance curves in Figure 4 are deviated from the ideal ones. This behavior can be explained in terms of anomalous diffusion:[19] a higher slope than unity is observed for semiinfinite diffusion when the diffusing species wait after each jump for a period drawn from a broad power-law distribution. The effect is that some diffusing species stick for a long time in the diffusion path and diffusion becomes slower. Using Eq. (8) and the values of the circuit elements, the values of the diffusion coefficient of aluminum ions in the graphite, D_{ion}, were obtained as 2.8×10^{-10} cm^2/s, which seems to be reasonable in solid state media.[20]

This behavior of the diffusion system means that the system is in a situation in which the number of diffusing particles is not conserved. No particular mesoscopic approach has validated this phenomenological generalization so far. It yields, however, interesting impedance properties, as we show in the following section. The constitutive equation remains the same, Eq. (1). In this generalization, the diffusion equation reads

$$\frac{\partial^{\gamma} c}{\partial t^{\gamma}} = D\frac{\partial^2 c}{\partial x^2}. \tag{13}$$

In this case, the particle flux is zero at the boundary.

$$\frac{\partial c}{\partial x} = 0 \quad (x = L) \tag{14}$$

Using the boundary condition of Eq. (5), the impedance ions are obtained.[19]

$$Z(s) = R_W(\omega_d/s)^{\gamma/2}\coth[(s/\omega_d)^{\gamma/2}] \tag{15}$$

At high frequency, the impedance can be approximated by

$$Z(s) = R_W(\omega_d/s)^{\gamma/2}. \tag{16}$$

For$\gamma < 1$, Eq. (16) gives a straight line inclined at less than 45° in the complex plot. At low frequency $(\omega < \omega_d)$, Eq. (15) is approximately equal to

$$(x = L)Z(s) = \frac{1}{3}R_w + Qs^{-\gamma}, \tag{17}$$

where $Q = R_w\omega_d^{\gamma}$. The first term in Eq. (17) is a series resistance; the second is a CPE.[21] Thus, at low frequencies, Eq. (17) also tends toward an inclined straight line in the complex plot, as seen in Figure 4. Comparing Eqs. (16) and (17), one notices that the power-law exponent at low frequencies is exactly double that at high frequency. These features are also found in a model for impedance of porous electrodes, in which transport is driven by drift in the electrical field.[22] In this case, the value of γ was obtained as 0.75 by fitting results of experimental data with Eq. (17).

At a DC potential of –1.22 V, the diffusion coefficient is the highest and the ion movement occurs at the highest rate. Therefore, the ion accumulation has a minor effect and the capacitance value of the electrode is the lowest. In this case, there is anomalous diffusion with the absorbing boundary, seen in Figure 5.

In this case, the concentration of the $AlCl_4^-$ at the boundary remains at the equilibrium level.

$$C = 0 \quad (x = L) \tag{18}$$

These standard conditions refer to a random walker absorbed, as in Eq. (18), upon encountering a wall at $(x = L)$.

By applying this boundary condition to Eq. (9), it follows that

$$Q = 3R_w\omega_d^{\gamma} Z(s)^{-1} = R_w(\omega_d/s)^{\gamma/2} \tanh[(s/\omega_d)^{\gamma/2}]. \tag{19}$$

The function is illustrated in Figure 4. The behavior at high frequency is again shown by Eq. (16). At low frequencies, $\omega < \omega_d$, the admittance can be written, approximately, as:

$$Z(s)^{-1} = \frac{1}{Rw} + \frac{1}{Qs^{-\gamma}}, \tag{20}$$

where $Q = 3R_w\omega_d^{\gamma}$. Eq. (20) is the parallel combination of a resistance and C_{dl}, giving a depressed arc in the complex plot at low frequency.

The impedance functions of anomalous diffusion with an absorbing boundary were previously suggested on a heuristic basis[23] and were used for fitting experimental spectra. Since the model was related to nonuniform diffusion, it is worth noting that the assumed diffusion equation is spatially uniform; it is rather the time dependence that is generalized. Nonetheless, it must be emphasized again that no particular mesoscopic foundation has been provided for this model of anomalous diffusion.

Conclusion

This electrochemical impedance spectroscopy study in molten basic $AlCl_3$-NaCl-KCl showed the control diffusion process for $AlCl_4^-$ anions. EIS studies show anomalous diffusion with totally blocking and totally absorbing boundary conditions for $AlCl_4^-$ anions in graphite working electrodes. The main criterion to identify the anomalous diffusion behavior of $AlCl_4^-$ anions is the slope of the high-frequency line (γ).

Acknowledgements

We gratefully acknowledge the support of this work by the K.N. Toosi University of Technology Research Council.

References

1. Macdonald, J. R., Ed. Impedance Spectroscopy, Wiley, New York, 1987.
2. Ramos-Barrado, J. R.; Galan-Montenegro, P.; Criado, C. *J. Chem. Phys.* **1996**, *105*, 2813-2815.
3. Ho, C.; Raistrick, I. D.; Huggins, R. A. *J. Electrochem. Soc.* **1998**, *127*, 343-350.
4. Jou, D.; Casa-Vazquez, J.; Lebon, G. *Extended Irreversible Thermodynamics*, Springer, Berlin, 1996.
5. Hsu, W. K.; Terrones, M.; Hare, J. P.; Terrones, H.; Kroto, H. W.; Walton, D. R. W. *Chem. Phys. Lett.* **1996**, *262*, 161-164.
6. Chen, G. Z.; Fan, X.; Luget, A.; Shaffer, M. S. P.; Fray, D. J.; Windle, A. H. *J. Electroanal. Chem.* **1998**, *446*, 1-6.
7. Grjotheim, K.; Mathiasovsky, K. *Acta Chem. Scand. A* **1980**, *34*, 666-670.
8. Berg, R. W.; Hjuler, H. A., Bjerrum, N. J. *Inorg. Chem.* **1984**, *23*, 557-565.
9. Jafarian, M.; Mahjani, M. G.; Gobal, F.; Danaee, I. *J. Electroanal. Chem.* **2006**, *588*, 190-196.
10. Heli, H.; Hajjizadeh, M.; Jabbari, A.; Moosavi-Movahedi, A. A. *Biosens. Bioelectron.* **2009**, *24*, 2328-2333.
11. Mahjani, M. G.; Ehsani, A.; Jafarian, M. *Synthetic Met.* **2010,** *160*, 1252-1258.
12. Ehsani, A.; Mahjani, M. G.; Jafarian, M.; Naeemy, A. *Prog. Org. Coat.* **2010**, *69*, 510-516.
13. Itaya, K.; Ataka, T.; Uchida, I.; Toshima, S. *J. Am. Chem. Soc.* **1982**, *104*, 4767-4772.
14. Gabrielli, C.; Keddam, M.; Nadi, N.; Perrot, H. *J. Electroanal. Chem.* **2000**, *485*, 101-113.
15. Barsoukov, E.; Macdonald, J. R. *Impedance Spectroscopy*, Wiley, New Jersey, 2005.
16. Pajkossy, T. *J. Electroanal. Chem.* **1994**, *364*, 111-125.
17. Neves, R. S.; Robertis, E. D.; Motheo, A. *Electrochim. Acta* **2006**, *51*, 1215-1224.
18. Gupta, V.; Kusahara, T.; Toyama, H.; Gupta, S.; Miura, N. *Electrochem. Commun.* **2007**, *9*, 2315-2319.
19. Bisquert, J.; Compte, A. *J. Electroanal. Chem.* **2001**, *499*, 112-120.
20. Wang, X.; Aoki, K. *J. Electroanal. Chem.* **2007**, *604*, 101-108.
21. Bisquert, J.; Garcia-Belmonte, G.; Fabregat-Santiago, F.; Bueno, P. R. *J. Electroanal. Chem.* **1999**, *475*, 152-163.
22. Bisquert, J.; Garcia-Belmonte, G.; Fabregat-Santiago, F.; Ferriols, N. S.; Bogdanoff, P.; Pereira, E. C. *J. Phys. Chem. B* **2000**, *104*, 2287-2298.
23. Cabanel, R.; Barral, G.; Diard, J.-P.; Le Gorrec, B.; Montella, C. *J. Appl. Electrochem.* **1993**, *23*, 93-97.